AIAA JOURNAL
Vol. 37, No. 7, July 1999

Discontinuous Time-Integration Method for Dynamic Contact/Impact Problems

Jin Yeon Cho* and Seung Jo Kim†
Seoul National University, Seoul 151-742, Republic of Korea

A new time-integration method is proposed using the generalized derivative concept to simulate the dynamic phenomena with sudden constraint occurring in dynamic contact/impact problems. By the adoption of the generalized derivative concept and the jump assumption, discontinuity can be incorporated in time integration, and as a result, the algorithm does not need any other special consideration of jumps in dynamic field variables due to sudden constraint, such as dynamic contact–release conditions. To observe the characteristics of the proposed time-integration method, stability and convergence analyses are carried out. The analyses prove that the proposed method with linear approximation in the time domain yields unconditional stability and third-order accuracy. In numerical tests, several dynamic contact/impact problems are analyzed by straightforward application of the proposed time-integration method with the exterior penalty method. From the tests, it is shown that the proposed time-integration method can be used successfully with the penalty method in numerical simulations of dynamic contact/impact problems.

I. Introduction

DYNAMIC contact/impact problems[1] are often encountered in mechanical and structural systems. Because the impact phenomena induce stiffness degradation and local failure in structural systems, the impact behavior of safety-related structural systems must be precisely analyzed. For example, the impact analysis of laminated composite structures is very important. Composite structures are susceptible to impact loading even though they have been used extensively in aerospace and the other applications due to their good material properties. Especially in the case of low-velocity impact[2,3] there may be significant internal damage resulting in a substantial drop in the stiffness and strength of the structures, although no apparent damage is detected by visual inspection, leading directly to safety-related problems of structures.

To simulate contact/impact problems, several studies have been carried out, and it has been pointed out that the impenetrability condition alone in the contact area is not sufficient in the numerical simulations of dynamic contact/impact problems. The sudden constraint induces the jumps in dynamic field variables, which makes it difficult to satisfy the velocity and the acceleration compatibility between the target and impactor under discrete time integration, such as the Newmark method.[4] As a result, straightforward application of the impenetrability condition without any other treatment produces undesirable oscillations. This is a somewhat different issue in solving static contact problems. To alleviate this problem, several studies were performed. Hughes et al.[5] devised the discrete dynamic contact/impact conditions for a lumped-mass case and enforced the conditions. Taylor and Papadopoulos[6] assumed that the velocities and accelerations on the contact points are independent of the displacements in the Newmark time-integration method and enforced the velocity and the acceleration compatibility. Chaudhary and Bathe[7] adopted the special parameters of the Newmark time-integration method to satisfy the momentum conservation principle of the isolated particle. Lee[8] proposed an iterative scheme for satisfying the velocity and the acceleration compatibility on the contact surface under the constant average acceleration method,[4] which is the Newmark method with $\delta = \frac{1}{2}$ and $\alpha = \frac{1}{4}$.

Several time-integration methods have been developed.[4,9] Each of these methods has its specialty for a specific problem. However, the methods may be inadequate for dynamic phenomena having a sudden constraint as in dynamic contact/impact problems and may need to focus on the treatment of jump discontinuity inasmuch as most of the time-integration methods are based on the continuous behavior in the time domain. Recently, some works were carried out to treat the second-order hyperbolic problems using the discontinuous Galerkin formulation.[10,11]

In this work, a new discontinuous time-integration method is presented to treat dynamic contact/impact problems. The proposed method uses the concept of the generalized derivative in distribution theory.[12,13] To observe the characteristics of the proposed method, stability and accuracy analyses are performed. By using the developed time-integration method along with the exterior penalty method, several numerical simulations of dynamic contact/impact problems are presented.

II. Discontinuous Time-Integration Method

A. Discrete Operator for Time Integration

As mentioned in the Introduction, the time-integration method is important in the analysis of dynamic contact/impact problems. The severe jumps in dynamic field variables produce undesirable oscillation. To alleviate this problem, it is reasonable to incorporate discontinuity in the development of the time-integration method. Toward this end, the concept of the generalized derivative in distribution theory and the jump assumption are considered together inasmuch as the definition of the generalized derivative can provide the meaning of the derivative even for a discontinuous distribution such as the Dirac delta function.[12] The definition of the generalized derivative of distribution[13] is constructed through an integration-by-parts formula. Using the procedure, the difficulty of differentiation of a distribution is transferred to the differentiation of a test function. Using the concept, a generalized relation between the displacement vector $\boldsymbol{u}(t)$ and velocity vector $\boldsymbol{v}(t)$ is constructed by the integration-by-parts formula:

$$\int_{t_0}^{t_f} \boldsymbol{w}^T \boldsymbol{v}\,\mathrm{d}t = -\int_{t_0}^{t_f} \dot{\boldsymbol{w}}^T \boldsymbol{u}\,\mathrm{d}t + \boldsymbol{w}^T \boldsymbol{u}\Big|_{t_0}^{t_f} \quad \text{for all} \quad \boldsymbol{w}(t) \qquad (1)$$

where $\boldsymbol{w}$ is the test function. It can be also regarded as the following weighted residual statement:

Received 14 March 1998; revision received 30 December 1998; accepted for publication 9 January 1999.

*Research Assistant, Department of Aerospace Engineering, San 56-1, Shillim-Dong, Kwanak-Ku; currently Postdoctoral Researcher, Center for Aerospace Research and Education, University of California, Los Angeles, Los Angeles, CA 90095-1600.

†Professor, Department of Aerospace Engineering, San 56-1, Shillim-Dong, Kwanak-Ku. Member AIAA.

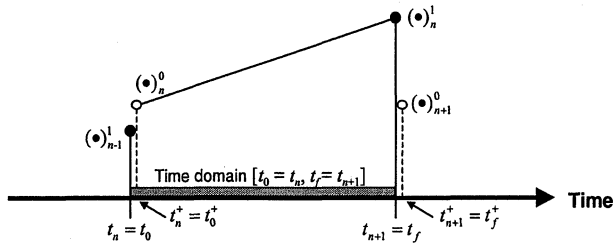

Fig. 1 Description of the time domain and jumps in dynamic variables.

$$0 = \int_{t_0}^{t_f} \boldsymbol{w}^T(\boldsymbol{v} - \dot{\boldsymbol{u}})\,\mathrm{d}t = \int_{t_0}^{t_f} \boldsymbol{w}^T\boldsymbol{v} + \dot{\boldsymbol{w}}^T\boldsymbol{u}\,\mathrm{d}t - \boldsymbol{w}^T\boldsymbol{u}\Big|_{t_0}^{t_f}$$

$$\text{for all} \quad \boldsymbol{w}(t) \qquad (2)$$

For the natural imposition of abrupt loading phenomena, the jump conditions at the initial time t_0 are assumed:

$$\boldsymbol{u}(t_0) \neq \boldsymbol{u}(t_0^+), \qquad \boldsymbol{v}(t_0) \neq \boldsymbol{v}(t_0^+) \qquad (3)$$

where superscript + is the right limit of time t_0 as shown in Fig. 1. As a result, relation (2) incorporates the jump due to the shock loading condition, using the jump conditions (3). In the same way, the acceleration–velocity relation is written as follows:

$$\int_{t_0}^{t_f} \boldsymbol{w}^T\boldsymbol{a}\,\mathrm{d}t = -\int_{t_0}^{t_f} \dot{\boldsymbol{w}}^T\boldsymbol{v}\,\mathrm{d}t + \boldsymbol{w}^T\boldsymbol{v}\Big|_{t_0}^{t_f} \qquad \text{for all} \quad \boldsymbol{w}(t) \qquad (4)$$

where

$$\boldsymbol{v}(t_0) \neq \boldsymbol{v}(t_0^+), \qquad \boldsymbol{a}(t_0) \neq \boldsymbol{a}(t_0^+)$$

where $\boldsymbol{a}$ is the acceleration vector. In contrast with dynamic field variables, i.e., $\boldsymbol{u}$, $\boldsymbol{v}$, and $\boldsymbol{a}$, test function $\boldsymbol{w}$ is assumed to be continuous at t_0 to enforce the effect of the initial condition.

For the temporal approximation, the time domain of the investigation is restricted to $[t_n = t_0, t_{n+1} = t_f]$, and the linear Lagrange interpolation functions in the time domain are used for approximating displacement $\boldsymbol{u}$, velocity $\boldsymbol{v}$, acceleration $\boldsymbol{a}$, and test function $\boldsymbol{w}$, as in finite element discretization. The approximation vectors defined on an interval $t_n < t \leq t_{n+1} = t + \Delta t$ are written in the following forms:

$$\begin{aligned} \boldsymbol{u}(t) &= \sum_{i=0}^{1} \psi_i(t)\boldsymbol{u}_n^i, & \boldsymbol{v}(t) &= \sum_{i=0}^{1} \psi_i(t)\boldsymbol{v}_n^i \\ \boldsymbol{a}(t) &= \sum_{i=0}^{1} \psi_i(t)\boldsymbol{a}_n^i, & \boldsymbol{w}(t) &= \sum_{i=0}^{1} \psi_i(t)\boldsymbol{w}_n^i \end{aligned} \qquad (5)$$

where $\psi_0(t) = (t_{n+1} - t)/(t_{n+1} - t_n)$ and $\psi_1(t) = (t - t_n)/(t_{n+1} - t_n)$. Here, $()_n^0$ and $()_n^1$ are field values at time t_n^+ and t_{n+1}, respectively (shown in Fig. 1). For a higher-order approximation, a higher-order interpolation function can be used, as by Kim et al.[14] By the substitution of interpolating functions (5) into Eqs. (2) and (4), approximated relations for the time derivative are obtained. The relations are written as follows through reordering:

For all $\boldsymbol{w}_n^i$ $(i = 0, 1)$,

$$\begin{aligned} &\sum_{j=0}^{1} \int_{t_n}^{t_{n+1}} \dot{\psi}_i\psi_j \boldsymbol{w}_n^{i\,T}\boldsymbol{u}_n^j\,\mathrm{d}t - \boldsymbol{w}^T\boldsymbol{u}\Big|_{t_{n+1}} \\ &\quad = -\sum_{j=0}^{1} \int_{t_n}^{t_{n+1}} \psi_i\psi_j \boldsymbol{w}_n^{i\,T}\boldsymbol{v}_n^j\,\mathrm{d}t - \boldsymbol{w}^T\boldsymbol{u}\Big|_{t_n} \\ &\sum_{j=0}^{1} \int_{t_n}^{t_{n+1}} \dot{\psi}_i\psi_j \boldsymbol{w}_n^{i\,T}\boldsymbol{v}_n^j\,\mathrm{d}t - \boldsymbol{w}^T\boldsymbol{v}\Big|_{t_{n+1}} \\ &\quad = -\sum_{j=0}^{1} \int_{t_n}^{t_{n+1}} \psi_i\psi_j \boldsymbol{w}_n^{i\,T}\boldsymbol{a}_n^j\,\mathrm{d}t - \boldsymbol{w}^T\boldsymbol{v}\Big|_{t_n} \end{aligned} \qquad (6)$$

where

$$\boldsymbol{u}(t_n) = \boldsymbol{u}_{n-1}^1, \qquad \boldsymbol{v}(t_n) = \boldsymbol{v}_{n-1}^1, \qquad \boldsymbol{a}(t_n) = \boldsymbol{a}_{n-1}^1$$

$$\boldsymbol{w}(t_n) = \boldsymbol{w}_n^0, \qquad \boldsymbol{u}(t_{n+1}) = \boldsymbol{u}_n^1, \qquad \boldsymbol{v}(t_{n+1}) = \boldsymbol{v}_n^1$$

$$\boldsymbol{a}(t_{n+1}) = \boldsymbol{a}_n^1, \qquad \boldsymbol{w}(t_{n+1}) = \boldsymbol{w}_n^1$$

In Eq. (6), the dynamic field variables $\boldsymbol{u}$, $\boldsymbol{v}$, and $\boldsymbol{a}$ contain the discontinuities at initial time t_0 $(= t_n)$, and $\boldsymbol{u}_{n-1}^1$, $\boldsymbol{v}_{n-1}^1$, and $\boldsymbol{a}_{n-1}^1$ are the given initial vectors obtained from the preceding time step. The effect of the initial condition is weakly imposed via $\boldsymbol{u}_{n-1}^1$, $\boldsymbol{v}_{n-1}^1$, and $\boldsymbol{a}_{n-1}^1$. Because Eq. (6) must hold for all $\boldsymbol{w}_n^i$, it can be written in simplified matrix form as

$$\hat{\Phi}\boldsymbol{U}_{n+1} = \Phi\boldsymbol{V}_{n+1} + \Theta\boldsymbol{U}_n, \qquad \hat{\Phi}\boldsymbol{V}_{n+1} = \Phi\boldsymbol{A}_{n+1} + \Theta\boldsymbol{V}_n \qquad (7)$$

where

$$\boldsymbol{U}_{n+1} = \{\boldsymbol{u}_n^{0T}, \boldsymbol{u}_n^{1T}\}^T, \qquad \boldsymbol{V}_{n+1} = \{\boldsymbol{v}_n^{0T}, \boldsymbol{v}_n^{1T}\}^T$$

$$\boldsymbol{A}_{n+1} = \{\boldsymbol{a}_n^{0T}, \boldsymbol{a}_n^{1T}\}^T$$

The alternative forms for displacement–velocity and velocity–acceleration relations are obtained by the inversion:

$$\begin{aligned} \boldsymbol{U}_{n+1} &= \bar{\Psi}\boldsymbol{V}_{n+1} + \bar{\Psi}_0\boldsymbol{V}_n + \boldsymbol{J}\boldsymbol{U}_n \\ \boldsymbol{V}_{n+1} &= \bar{\Psi}\boldsymbol{A}_{n+1} + \bar{\Psi}_0\boldsymbol{A}_n + \boldsymbol{J}\boldsymbol{V}_n \end{aligned} \qquad (8)$$

where $\bar{\Psi} = \hat{\Phi}^{-1}\Phi$, $\bar{\Psi}_0 = \boldsymbol{0}$, and $\boldsymbol{J} = \hat{\Phi}^{-1}\Theta$. Using the discrete operators of Eq. (8), a numerical time-integration algorithm is constructed with the dynamic equilibrium equation.

B. Numerical Time-Integration Algorithm

The dynamic equilibrium equation of a dynamic system discretized in the space domain is given as follows:

$$\boldsymbol{m}\boldsymbol{a} + \boldsymbol{c}\boldsymbol{v} + \boldsymbol{k}\boldsymbol{u} = \boldsymbol{f} \qquad (9)$$

where $\boldsymbol{m}$, $\boldsymbol{c}$, and $\boldsymbol{k}$ are mass, damping, and stiffness matrices, respectively. The external force vector is $\boldsymbol{f}$. With the obtained discrete operator (8), the dynamic equilibrium equations at the inner time steps, i.e., t_n^+ and t_{n+1}, are considered to obtain a time-integration algorithm:

$$\boldsymbol{m}\boldsymbol{a}_n^i + \boldsymbol{c}\boldsymbol{v}_n^i + \boldsymbol{k}\boldsymbol{u}_n^i = \boldsymbol{f}_n^i \qquad (i = 0, 1) \qquad (10)$$

Using the matrix notation, it can be written as

$$\boldsymbol{M}\boldsymbol{A}_{n+1} + \boldsymbol{C}\boldsymbol{V}_{n+1} + \boldsymbol{K}\boldsymbol{U}_{n+1} = \boldsymbol{F}_{n+1} \qquad (11)$$

where $\boldsymbol{M}$, $\boldsymbol{C}$, and $\boldsymbol{K}$ are block diagonal matrices for mass, damping, and stiffness, respectively, and $\boldsymbol{F}_{n+1}$ is the forcing vector. To obtain the dynamic field variables $\boldsymbol{A}_{n+1}$, $\boldsymbol{V}_{n+1}$, and $\boldsymbol{U}_{n+1}$, it is sufficient to solve Eqs. (8) and (11) simultaneously. As a result, the numerical time-integration algorithm is reduced to solving the following system of algebraic equations:

For the given initial conditions $\boldsymbol{A}_n$, $\boldsymbol{V}_n$, and $\boldsymbol{U}_n$, find $\boldsymbol{A}_{n+1}$, $\boldsymbol{V}_{n+1}$, and $\boldsymbol{U}_{n+1}$ of the next time step such that

$$\begin{aligned} \boldsymbol{U}_{n+1} &= \bar{\Psi}\boldsymbol{V}_{n+1} + \bar{\Psi}_0\boldsymbol{V}_n + \boldsymbol{J}\boldsymbol{U}_n \\ \boldsymbol{V}_{n+1} &= \bar{\Psi}\boldsymbol{A}_{n+1} + \bar{\Psi}_0\boldsymbol{A}_n + \boldsymbol{J}\boldsymbol{V}_n \\ \boldsymbol{M}\boldsymbol{A}_{n+1} &+ \boldsymbol{C}\boldsymbol{V}_{n+1} + \boldsymbol{K}\boldsymbol{U}_{n+1} = \boldsymbol{F}_{n+1} \end{aligned} \qquad (12)$$

Like other methods, the system of algebraic equations for time-stepping numerical integration can be solved by several procedures, such as the predictor–corrector form. The detailed algorithm construction procedure is similar to that of Kim et al.[14] The predictor–corrector algorithm based on displacement form can be written as follows:

1) Calculate $\boldsymbol{a}_0$ such that $\boldsymbol{m}\boldsymbol{a}_0 + \boldsymbol{c}\boldsymbol{v}_0 + \boldsymbol{k}\boldsymbol{u}_0 = \boldsymbol{f}_0$. Set

$$\boldsymbol{A}_0 = \{\boldsymbol{0}^T, \boldsymbol{a}_0^T\}^T, \qquad \boldsymbol{V}_0 = \{\boldsymbol{0}^T, \boldsymbol{v}_0^T\}^T, \qquad \boldsymbol{U}_0 = \{\boldsymbol{0}^T, \boldsymbol{u}_0^T\}^T$$

2) Calculate $\boldsymbol{K}^{\text{eff}} = \boldsymbol{M}\bar{\Psi}^{-2} + \boldsymbol{C}\bar{\Psi}^{-1} + \boldsymbol{K}$ and $\boldsymbol{K}^{\text{eff}^{-1}}$.

3) With the initial condition A_n, V_n, and U_n obtained in the preceding time step, find A_{n+1}, V_{n+1}, and U_{n+1} of the next time step until the required time step, using the following procedure:
Predict

$$\tilde{A}_{n+1}^{(u)} = -\bar{\Psi}^{-1}\bar{\Psi}_0 A_n - \left(\bar{\Psi}^{-2}\bar{\Psi}_0 + \bar{\Psi}^{-1}J\right)V_n - \bar{\Psi}^{-2}JU_n$$
$$\tilde{V}_{n+1}^{(u)} = -\bar{\Psi}^{-1}\bar{\Psi}_0 V_n - \bar{\Psi}^{-1}JU_n \tag{13}$$

Calculate

$$R_{n+1}^{(u)} = F_{n+1} - M\tilde{A}_{n+1}^{(u)} - C\tilde{V}_{n+1}^{(u)}, \qquad U_{n+1} = K^{\text{eff}^{-1}} R_{n+1}^{(u)} \tag{14}$$

Correct

$$A_{n+1} = \tilde{A}_{n+1}^{(u)} + \bar{\Psi}^{-2}U_{n+1}, \qquad V_{n+1} = \tilde{V}_{n+1}^{(u)} + \bar{\Psi}^{-1}U_{n+1} \tag{15}$$

where $\tilde{A}_{n+1}^{(u)}$ and $\tilde{V}_{n+1}^{(u)}$ are predictors for acceleration and velocity, respectively. After the initialization and predictor stages, the displacements are obtained via Eq. (14). The acceleration and velocity are corrected by the correction equation (15). The algorithm needs only one correction.

C. Stability and Accuracy Analysis

By simple algebraic manipulations, Eqs. (8) and (14) can be rewritten as the following form, which does not contain the acceleration vector:

$$\begin{bmatrix} K^{\text{eff}} & 0 \\ I & -\bar{\Psi} \end{bmatrix} \begin{Bmatrix} U_{n+1} \\ V_{n+1} \end{Bmatrix} = \begin{bmatrix} \Xi_U & \Xi_V \\ J & \bar{\Psi}_0 \end{bmatrix} \begin{Bmatrix} U_n \\ V_n \end{Bmatrix} + \begin{Bmatrix} F_{n+1} + \bar{\Psi}^{-1}\bar{\Psi}_0 F_n \\ 0 \end{Bmatrix} \tag{16}$$

where $\Xi_U = M\bar{\Psi}^{-2}J + C\bar{\Psi}^{-1}J - K\bar{\Psi}^{-1}\bar{\Psi}_0$ and $\Xi_V = M(\bar{\Psi}^{-2}\bar{\Psi}_0 + \bar{\Psi}^{-1}J)$. I and $\mathbf{0}$ are the identity matrix and the null matrix, respectively. Equation (16) is written in simplified matrix form as

$$T\chi(t_{n+1}) = T_0\chi(t_n) + L(t_n, t_{n+1}) \tag{17}$$

where $T^{-1}T_0$ are the amplification of the displacement and velocity as time goes from t_n to t_{n+1} and L is the loading during the time interval $[t_n, t_{n+1}]$ in a generalized sense.

For the stability analysis, consider a single-degree-of-freedom system that excludes the damping and the applied loading condition. Then the system reduces to

$$\hat{T}\chi(t_{n+1}) = \hat{T}_0\chi(t_n) \tag{18}$$

When damping matrix C is equal to zero, T and T_0 reduce to $\hat{T}$ and $\hat{T}_0$, respectively. To find the amplification factor, it is sufficient to solve the following generalized eigenvalue problem: Find λ and χ such that

$$\lambda\hat{T}\chi = \hat{T}_0\chi \tag{19}$$

To guarantee the unconditional stability of the time-integration algorithm, all of the magnitudes of the amplification factors of the algorithm, i.e., magnitudes of the eigenvalues, must be less than or equal to 1. Figure 2 shows the magnitude of the eigenvalue (spectral radius). In Fig. 2, the proposed method is shown to be unconditionally stable because all of the magnitudes of the amplification factors are less than or equal to 1. Moreover, the method decays out the high-frequency responses compared to time step Δt, i.e., $\Delta t/T > 1$, because the amplification factor is zero in that region. This property gives the filtering effect of high-frequency noise.

To observe the accuracy of the proposed time-integration method, the free-oscillation problem with unit mass and stiffness is solved, and the amplitude decay error and period elongation error[4,15] are shown in Fig. 3. The slope of the curve is the order of convergence.

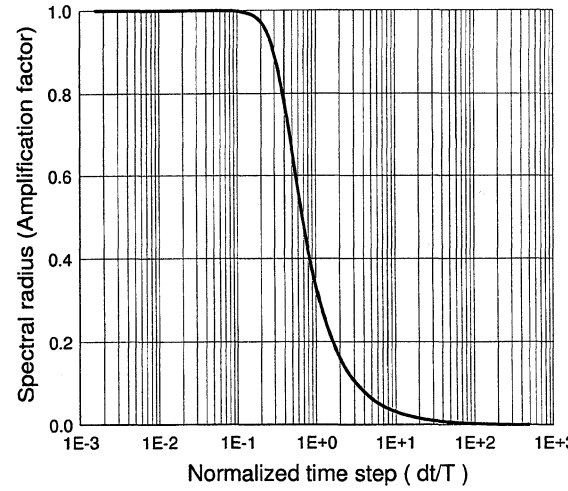

Fig. 2 Spectral radius vs normalized time step.

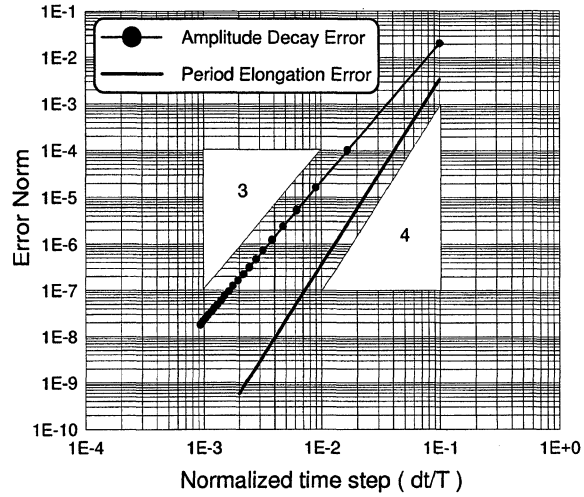

Fig. 3 Log-scale plot of error norm vs normalized time step.

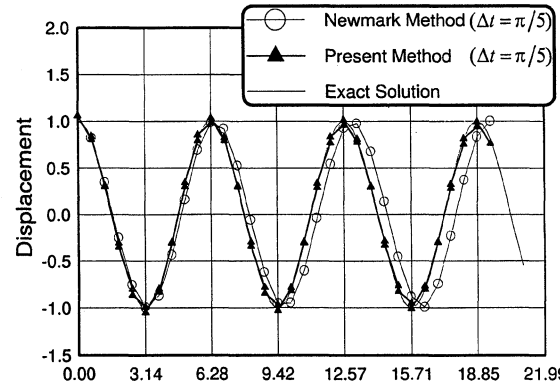

Fig. 4 Time-domain responses using the present method vs Newmark constant average acceleration method.

The results show that the proposed method has the third-order convergence in amplitude and fourth-order convergence in period if linear approximations are adopted in the time domain. Thus, it can be concluded that the proposed method with linear approximation in the time domain has third-order convergence at least, in combined cases, and is more accurate than the Newmark constant average acceleration method, which has second-order convergence.[14] In Fig. 4, the time-domain response of the free-oscillation system is given and compared with the exact solution and the result obtained by the Newmark constant average acceleration. Figure 4 clearly shows that the proposed method is much more accurate than the Newmark constant average acceleration method.

III. Dynamic Contact/Impact Problems

A. Variational Formulation of Dynamic Contact/Impact Problem

Consider an elastic body Ω with a boundary Γ impacted by a rigid body R in two-dimensional space. Then the dynamic process of the system is described by the following governing equations for each body. For the elastic body, the dynamic equilibrium equation is written as follows:

$$\rho\ddot{\boldsymbol{d}} - \nabla\cdot\boldsymbol{\sigma} = \boldsymbol{b} \qquad \text{in } \Omega \tag{20}$$

with boundary conditions $\boldsymbol{d}=\bar{\boldsymbol{d}}$ on Γ_D and $\boldsymbol{t}=\bar{\boldsymbol{t}}$ on Γ_F and with initial conditions $\boldsymbol{d}(\boldsymbol{x},0)=\boldsymbol{d}_0(\boldsymbol{x})$, $\dot{\boldsymbol{d}}(\boldsymbol{x},0)=\dot{\boldsymbol{d}}_0(\boldsymbol{x})$ for $\boldsymbol{x}\in\Omega$, where ρ is density, $\boldsymbol{d}$ is displacement, $\boldsymbol{\sigma}$ is stress, $\boldsymbol{b}$ is body force, and $\boldsymbol{t}$ is traction. Subscripts D and F are displacement boundary and force boundary, respectively. For the rigid body, the planar equations of motion have the following forms:

$$m_R\ddot{\boldsymbol{q}} = \boldsymbol{f}_R, \qquad I_R\ddot{\theta} = N_R \tag{21}$$

with initial conditions $\boldsymbol{q}(0)=\boldsymbol{q}_0, \dot{\boldsymbol{q}}(0)=\dot{\boldsymbol{q}}_0, \theta(0)=\theta_0$, and $\dot{\theta}(0)=\dot{\theta}_0$, where m_R, $\boldsymbol{q}$, and $\boldsymbol{f}_R$ are mass, displacement, and applied force of the rigid body, respectively. I_R, θ, and N_R are moment of inertia, rotation angle, and applied moment, respectively. The impenetrability condition[16] on the contact surface can be written by the inequality

$$\boldsymbol{d}\cdot\boldsymbol{n} \le s(\boldsymbol{x},\boldsymbol{q},\theta) \qquad \text{on } \Gamma_C \tag{22}$$

where $\boldsymbol{n}$ is the outward unit normal vector on Γ_C and s is the contact gap. In the contact boundary, the normal traction component is negative if there is contact. The tangential traction vector on the contact boundary is zero with the assumption of no friction. The variational form is derived from the principle of virtual work. In the variational formulation, both the rigid impactor and the solid target are incorporated, and penalized virtual work from the exterior penalty method[3,16] is added to satisfy the contact condition. The penalized external virtual work assumes the form

$$-\frac{1}{\varepsilon_p}\int_{\Gamma_C}(\boldsymbol{d}\cdot\boldsymbol{n}-s)^+\boldsymbol{n}\cdot\delta\boldsymbol{d}\,\mathrm{d}S + \frac{1}{\varepsilon_p}\int_{\Gamma_C}(\boldsymbol{d}\cdot\boldsymbol{n}-s)^+\frac{\mathrm{d}s}{\mathrm{d}\boldsymbol{q}}\cdot\delta\boldsymbol{q}\,\mathrm{d}S + \frac{1}{\varepsilon_p}\int_{\Gamma_C}(\boldsymbol{d}\cdot\boldsymbol{n}-s)^+\frac{\mathrm{d}s}{\mathrm{d}\theta}\delta\theta\,\mathrm{d}S \tag{23}$$

where $\psi^+(\boldsymbol{x})=\max\{\psi(\boldsymbol{x}),0\}$ is a nondifferentiable function and ε_p is a penalty parameter. Then the equilibrium equation can be written in the following variational form:

$$\begin{aligned}&\int_\Omega \rho\ddot{\boldsymbol{d}}\cdot\delta\boldsymbol{d}\,\mathrm{d}\Omega + \int_\Omega \boldsymbol{\sigma}\cdot\delta\boldsymbol{\varepsilon}\,\mathrm{d}\Omega - \int_\Omega \boldsymbol{b}\cdot\delta\boldsymbol{d}\,\mathrm{d}\Omega \\ &- \int_{\Gamma_F}\bar{\boldsymbol{t}}\cdot\delta\boldsymbol{d}\,\mathrm{d}S + (m_R\ddot{\boldsymbol{q}}-\boldsymbol{f}_R)\cdot\delta\boldsymbol{q} + (I_R\ddot{\theta}-N_R)\delta\theta \\ &+ \frac{1}{\varepsilon_p}\left[\int_{\Gamma_C}(\boldsymbol{d}\cdot\boldsymbol{n}-s)^+\boldsymbol{n}\cdot\delta\boldsymbol{d}\,\mathrm{d}S - \int_{\Gamma_C}(\boldsymbol{d}\cdot\boldsymbol{n}-s)^+\frac{\mathrm{d}s}{\mathrm{d}\boldsymbol{q}}\cdot\delta\boldsymbol{q}\,\mathrm{d}S \right.\\ &\left. - \int_{\Gamma_C}(\boldsymbol{d}\cdot\boldsymbol{n}-s)^+\frac{\mathrm{d}s}{\mathrm{d}\theta}\delta\theta\,\mathrm{d}S\right] = 0\end{aligned} \tag{24}$$

The variational form can be also derived from Hamilton's principle with the penalized energy. The penalty terms in Eq. (24) make the problem nonlinear. The normal traction component on the contact boundary can be obtained by

$$\boldsymbol{n}\cdot\boldsymbol{\sigma}\cdot\boldsymbol{n} = -(1/\varepsilon_p)(\boldsymbol{d}\cdot\boldsymbol{n}-s)^+ \tag{25}$$

B. Finite Element Approximation and Application of Time Integration

For the finite element approximation, the coordinate $\boldsymbol{x}$ and displacement $\boldsymbol{d}$ in an element are interpolated by an n-node isoparametric plane strain element:

$$\boldsymbol{x} = \begin{bmatrix}X\\Y\end{bmatrix} = \sum_{i=1}^{n}\phi_i\boldsymbol{x}_i = \boldsymbol{H}\boldsymbol{x}_e, \qquad \boldsymbol{d} = \begin{bmatrix}d_X\\d_Y\end{bmatrix} = \sum_{i=1}^{n}\phi_i\boldsymbol{u}_i = \boldsymbol{H}\boldsymbol{u}_e \tag{26}$$

From the strain-displacement relation and Eq. (26), the strains in an element are given by

$$\boldsymbol{\varepsilon} = \sum_{i=1}^{n}\boldsymbol{B}_i\boldsymbol{u}_i = \boldsymbol{B}\boldsymbol{u}_e \tag{27}$$

Using Eqs. (24), (26), and (27) with the linear elastic constitutive relation, the discretized equation can be obtained by assembling the element matrices and the equation of the rigid impactor:

$$\boldsymbol{m}\ddot{\boldsymbol{u}} + [\boldsymbol{k} + (1/\varepsilon_p)\boldsymbol{k}_N(\boldsymbol{u})]\boldsymbol{u} = \boldsymbol{f} + (1/\varepsilon_p)\boldsymbol{f}_N(\boldsymbol{u}) \tag{28}$$

where $\boldsymbol{u}$ is the global displacement vector and $\boldsymbol{m}$, $\boldsymbol{k}$, and $\boldsymbol{f}$ are the global mass, stiffness matrices, and force vector, respectively. The trapezoidal rule[16] is used instead of the Gauss quadrature rule in the numerical integration of $\boldsymbol{k}_N$ and $\boldsymbol{f}_N$. To obtain the time-dependent behavior of the dynamic system, the discretized governing equation (28) is integrated directly by the developed time-integration method in the preceding section without additional constraint such as the contact–release condition or special modification. The equilibrium equations at the inner time step i of the time interval $[t_n, t_{n+1}]$ are written as

$$\boldsymbol{m}\boldsymbol{a}_n^i + \left[\boldsymbol{k} + (1/\varepsilon_p)\boldsymbol{k}_N(\boldsymbol{u}_n^i)\right]\boldsymbol{u}_n^i = \boldsymbol{f}_n^i + (1/\varepsilon_p)\boldsymbol{f}_N(\boldsymbol{u}_n^i), \qquad i=0,1 \tag{29}$$

In matrix form, it is rewritten by using the notation of the preceding section:

$$\boldsymbol{M}\boldsymbol{A}_{n+1} + [\boldsymbol{K} + \boldsymbol{K}_N(\boldsymbol{U}_{n+1})]\boldsymbol{U}_{n+1} = \boldsymbol{F}_{n+1} + \boldsymbol{F}_N(\boldsymbol{U}_{n+1}) \tag{30}$$

For the time integration, it is sufficient to solve the system of equations as follows:

For the given initial conditions $\boldsymbol{A}_n$, $\boldsymbol{V}_n$, and $\boldsymbol{U}_n$, find $\boldsymbol{A}_{n+1}$, $\boldsymbol{V}_{n+1}$, and $\boldsymbol{U}_{n+1}$ of the next time step such that

$$\begin{aligned}\boldsymbol{U}_{n+1} &= \bar{\Psi}\boldsymbol{V}_{n+1} + \bar{\Psi}_0\boldsymbol{V}_n + \boldsymbol{J}\boldsymbol{U}_n \\ \boldsymbol{V}_{n+1} &= \bar{\Psi}\boldsymbol{A}_{n+1} + \bar{\Psi}_0\boldsymbol{A}_n + \boldsymbol{J}\boldsymbol{V}_n \\ \boldsymbol{M}\boldsymbol{A}_{n+1} &+ [\boldsymbol{K} + \boldsymbol{K}_N(\boldsymbol{U}_{n+1})]\boldsymbol{U}_{n+1} = \boldsymbol{F}_{n+1} + \boldsymbol{F}_N(\boldsymbol{U}_{n+1})\end{aligned} \tag{31}$$

As a result, direct application of the proposed time-integration method to Eq. (29) yields the following fully discretized dynamic equilibrium equation:

$$[\hat{\boldsymbol{K}} + \boldsymbol{K}_N(\boldsymbol{U}_{n+1})]\boldsymbol{U}_{n+1} = \hat{\boldsymbol{F}}_{n+1} + \boldsymbol{F}_N(\boldsymbol{U}_{n+1}) \tag{32}$$

where $\hat{\boldsymbol{K}} = \boldsymbol{M}\bar{\Psi}^{-2} + \boldsymbol{K}$ and $\hat{\boldsymbol{F}}_{n+1} = \boldsymbol{F}_{n+1} + \boldsymbol{M}[\bar{\Psi}^{-1}\bar{\Psi}_0\boldsymbol{A}_n + (\bar{\Psi}^{-2}\bar{\Psi}_0 + \bar{\Psi}^{-1}\boldsymbol{J})\boldsymbol{V}_n + \bar{\Psi}^{-2}\boldsymbol{J}\boldsymbol{U}_n]$.

To solve the system of nonlinear algebraic equations, the successive iteration scheme[9] is used. Application of the successive iteration scheme yields the system of equations for iteration as follows:

$$\left[\hat{\boldsymbol{K}} + \boldsymbol{K}_N\left(\boldsymbol{U}_{n+1}^{(k-1)}\right)\right]\boldsymbol{U}_{n+1}^{(k)} = \hat{\boldsymbol{F}}_{n+1} + \boldsymbol{F}_N\left(\boldsymbol{U}_{n+1}^{(k-1)}\right) \tag{33}$$

where k is the iteration number in each time step. Relative error of displacement is used as convergence criterion, where

$$\text{relative error} = \begin{cases}\left\|\boldsymbol{U}_{n+1}^{(k)} - \boldsymbol{U}_{n+1}^{(k-1)}\right\| / \left\|\boldsymbol{U}_{n+1}^{(k)}\right\| & \text{if } \left\|\boldsymbol{U}_{n+1}^{(k)}\right\| \neq 0 \\ \left\|\boldsymbol{U}_{n+1}^{(k)} - \boldsymbol{U}_{n+1}^{(k-1)}\right\| & \text{if } \left\|\boldsymbol{U}_{n+1}^{(k)}\right\| = 0\end{cases} \tag{34}$$

Iteration is carried out until the relative error is less than the given tolerance 10^{-6}.

IV. Numerical Simulations

By the developed computer code based on the fully discretized equation (32), several dynamic contact/impact problems are computed. In the numerical simulations, the selected examples are compared with the results of the Newmark constant average acceleration method to show the accuracy and stability of the proposed algorithm.

A. Bar Impact

To check the validity of the developed code for analyzing the dynamic contact/impact problem, the typical bar impact problem in

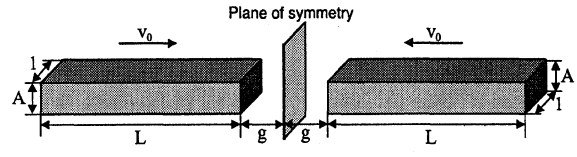

Fig. 5 Impact of two identical bars.

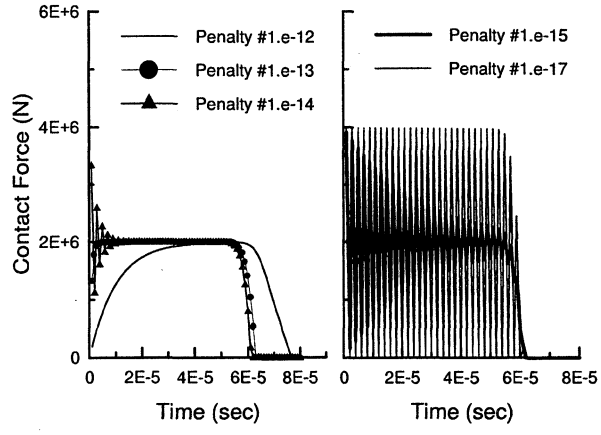

a) 1-μs time step

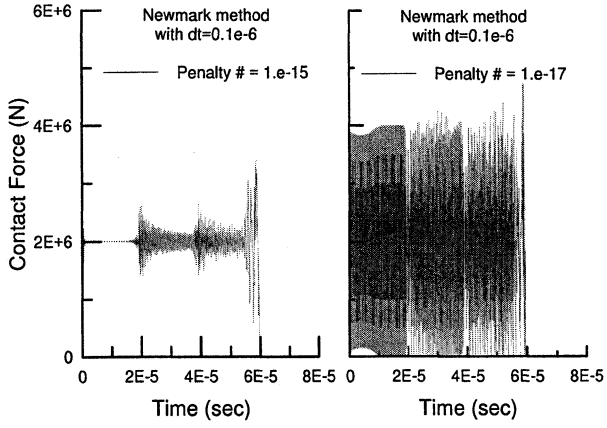

b) 0.1-μs time step

Fig. 6 Contact force history of bar impact using the Newmark constant average acceleration method.

Fig. 5 is analyzed. The results are compared with the analytic solution in Ref. 1 Here, 200 plane strain elements (four-node isoparametric elements) are used. Except for the simulation in Fig. 6b, a time step of 1 μs is used in the simulations. Because the problem has a symmetric nature, one side of the impact bar is discretized. The material properties and the dimensions for the problem are as follows: $E = 100$ GPa, $A = 2$ cm, $g = 0$ cm, $\rho = 1000$ kg/m^3, $L = 30$ cm, and $v_0 = 10$ m/s, where E is Young's modulus, A is thickness (cross-sectional area per unit length), g is initial gap, L is length, and v_0 is initial velocity of the bar. In the simulation of bar impact, Poisson's ratio ν is set to be 0. The contact force obtained by the analytical method is 2×10^6 N at $0 \leq t \leq 60$ μs and zero at $t > 60$ μs.

The contact force histories shown in Fig. 6 are the results of computation by the direct application of the Newmark constant average acceleration method for several penalty parameters. From the results, it is observed that the direct use of the Newmark constant average acceleration method without additional constraint, such as contact–release condition, produces undesirable oscillation.[8] It is also observed that the oscillation increases as the penalty parameter is decreased.[17] Even though a much smaller time step is used with the Newmark constant average acceleration method, it is very difficult to eliminate the undesirable oscillation. The results obtained by the Newmark constant average acceleration method with a smaller time step are presented in Fig. 6b. The time step adopted in Fig. 6b is 0.1 μs, that is, $\frac{1}{10}$th of the time step used in Figs. 6a and 7. Figure 6b

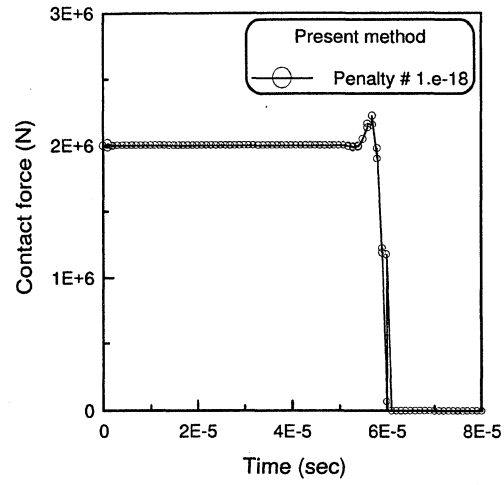

Fig. 7 Contact force history of bar impact using the present time-integration method with 1-μs time step.

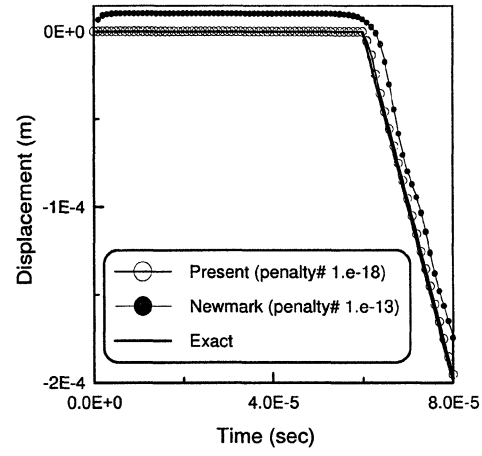

Fig. 8 Displacement history of contact node (bar impact) with 1-μs time step.

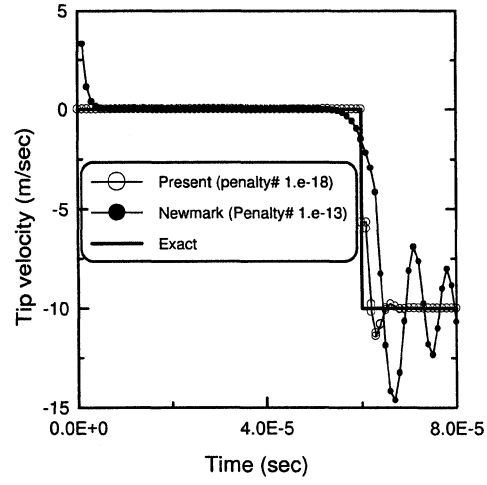

Fig. 9 Velocity history of contact node (bar impact) with 1-μs time step.

clearly shows that spurious oscillation cannot be easily eliminated even if a much smaller time step is used with Newmark constant average acceleration with a penalty-based contact algorithm. It is noted that widely used explicit methods, such as the central difference method with a penalty contact algorithm, also induces undesirable oscillation.[17] However, the direct use of the proposed method gives a stable solution in spite of the smaller penalty parameter of $1e-18$, as shown in Fig. 7. In Figs. 8 and 9, the displacement and the velocity of the contact node are plotted. For the Newmark case,

the results of the penalty parameter of $1e-13$ are presented because the contact force of that case is not oscillatory. The result in Fig. 8 shows that penetration occurs in the Newmark case; however, the proposed method does not allow the penetration. It is observed in Fig. 9 that the proposed method successfully describes the velocity jump at time $t=0$. From the results, it can be verified that the proposed method is adequate in dynamic contact/impact problems.

B. Impact of Isotropic Solid with Rigid Cylinder

As the second example, the impact behavior of a solid block with a rigid cylinder is simulated by both the Newmark constant average acceleration method and the proposed method. The material properties and the dimensions for the model problem are as follows: $\rho=2710$ kg/m^3, $E=70$ GPa, $\nu=0.3$, $L=3$ cm, $A=1$ cm, $m=65.8$ g, $v_0=10$ m/s, and $R=1$ cm, where m is the mass of the impactor, v_0 is the initial velocity of the impactor, and R is the radius of the impactor. The total number of nodes in the finite element model is 1681, and the element number is 1600. For time integration, a 0.2-μs time step size is used. The bottom is fixed in the y direction, and both sides are fixed in the x direction. In the simulation, the symmetric condition is utilized. The finite element model used in the analysis is shown in Fig. 10. Figure 11 shows the contact force history. It is observed that the results obtained by the Newmark method show numerical instability in the penalty parameter of $1e-16$, whereas the proposed method gives a stable solution in the smaller penalty parameter of $1e-18$. The displacement and the velocity of the rigid cylinder (impactor) and contact node (target) are shown in Figs. 12 and 13, respectively. Direct application of the Newmark method allows penetration in the penalty parameter of $1e-15$, which gives feasible contact force. Moreover, it produces undesirable oscillation in the velocity field. However, the impenetrability condition and velocity compatibility at the contact region are precisely satisfied by the proposed method. Especially if the proposed method is used, the velocity jump at the outset of impact is numerically realized due to the intrinsic formulation containing the jump discontinuity.

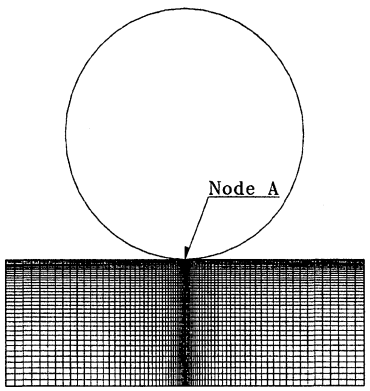

Fig. 10 Finite element model of solid block.

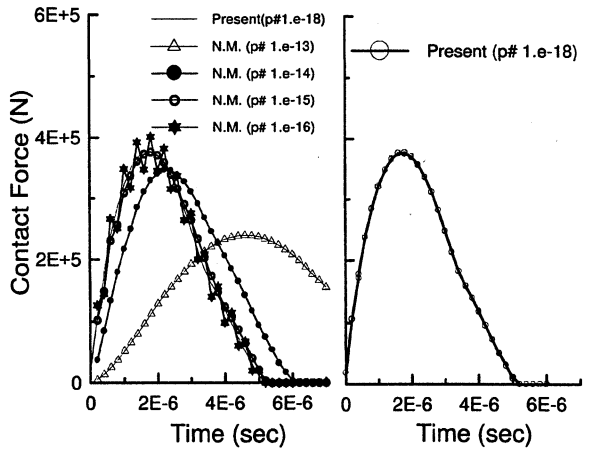

Fig. 11 Contact force history according to impact between solid block and rigid cylinder.

Table 1 Properties of composite materials

Property	Value
E_1	145.4 GPa
E_2	9.997 GPa
G_{12}	5.689 GPa
ν_{12}	0.3
ν_{23}	0.3
ρ	1536 kg/m^3

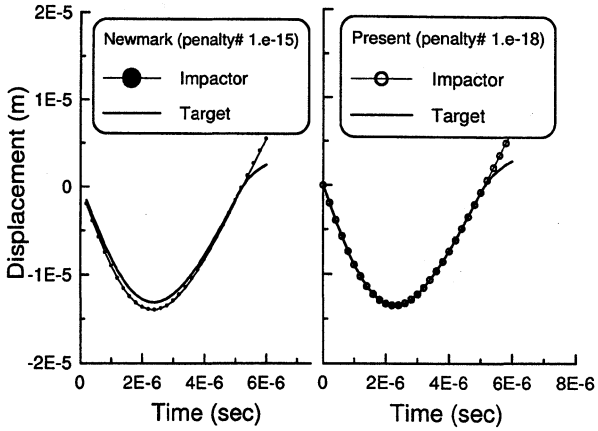

Fig. 12 Displacement histories of contact node A (target) and rigid cylinder (impactor).

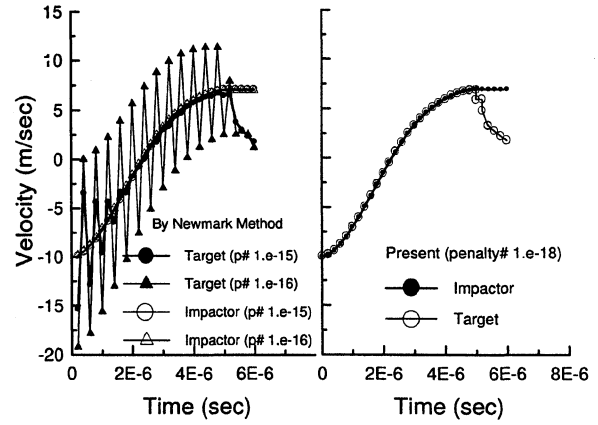

Fig. 13 Velocity histories of contact node A (target) and rigid cylinder (impactor).

C. Impact of Circular Composite Structures with Rigid Cylinder

As a final example, a simply supported circular composite structure under impact loading is analyzed by the proposed method. The lamination pattern of the composite structure is $[90_3/0_3/0_3/90_3]$. The material properties of the composite are shown in Table 1. The dimensions for the model problem are as follows: $R_c=2.5$ cm, $A=2.54$ mm, $m=10$ g, $v_0=10$ cm/s, and $R=6$ mm, where R_c is the inner radius of the composite structure. The total number of nodes is 793, and the element number is 720. For time integration, a 2-μs time step size is used. In the simulation, $1e-18$ is adopted as the penalty parameter. The finite element model used in the analysis is shown in Fig. 14. Because of the symmetry of the shape, a half-model is used with the symmetry condition. The contact force history is presented in Fig. 15. In contrast to the isotropic case, the contact force history is not smooth because the stress wave is reflected and transmitted complexly at the interface of different layers. Displacement and velocity histories are shown in Figs. 16 and 17, respectively. As with the first two examples, the impenetrability and velocity compatibility conditions are nicely satisfied during the contacting periods.

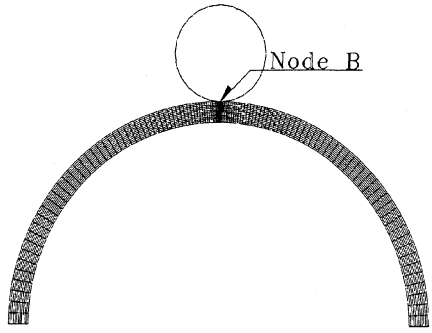

Fig. 14 Finite element model of circular composite structure.

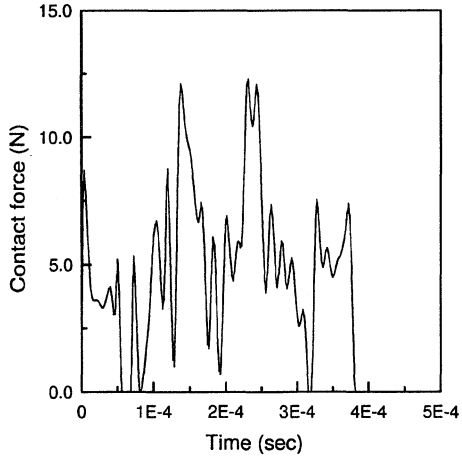

Fig. 15 Contact force history using the proposed time-integration method.

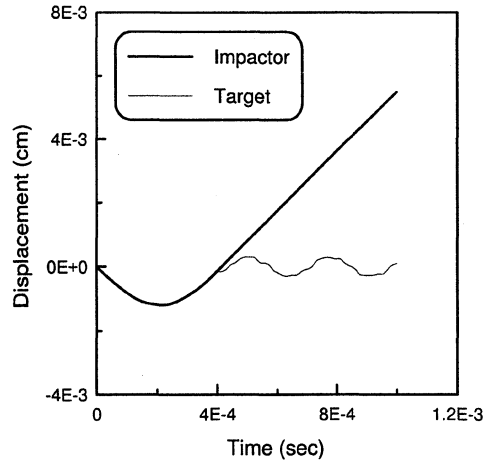

Fig. 16 Displacement histories of contact node B in circular composite structure and impactor using the proposed time-integration method.

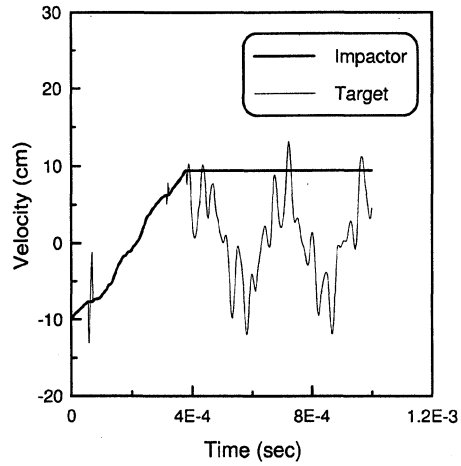

Fig. 17 Velocity histories of contact node B in circular composite structure and impactor using the proposed time-integration method.

V. Conclusion

A new time-integration algorithm for dynamic phenomena having a sudden constraint occurring in dynamic contact/impact analysis is developed using the concept of the generalized derivative. Using the generalized derivative concept and jump assumption, the jump discontinuity can be naturally incorporated in numerical time integration.

To observe the characteristics of the proposed time-integration method, stability and convergence analyses are carried out. The stability analysis proves that the proposed method gives unconditional stability and decays out the high-frequency noise. From the convergence analysis, it is concluded that the proposed method has third-order accuracy, at least, if the linear approximation is adopted in the time domain. In the numerical examples, several dynamic contact/impact problems are analyzed by straightforward application of the proposed time-integration method with the exterior penalty method. The selected simulation results are compared with the results of computation using the Newmark constant average acceleration method. From the tests, it has been verified that direct use of the Newmark constant average acceleration method produces undesirable oscillation, as noted in previous works; however, the proposed time-integration method can be used successfully in the numerical simulations of dynamic contact/impact phenomena without additional constraint except for the impenetrability condition. Thus, it is concluded that the dynamic phenomena with sudden constraint can be efficiently treated by using the proposed time-integration method.

Acknowledgments

The authors would like to acknowledge the financial support from the Agency for Defense Development, Republic of Korea, under Contract UD980011AD and the Systems Engineering Research Institute Supercomputer Center Cray Research and Development Grant Program.

References

[1]Goldsmith, W., *Impact*, Edward Arnold, London, 1960, Chaps. 1 and 3.

[2]Abrate, S., "Impact on Laminated Composite Materials," *Applied Mechanics Reviews*, Vol. 44, No. 4, 1991, pp. 155–190.

[3]Goo, N. S., and Kim, S. J., "Dynamic Contact Analysis of Laminated Composite Plates Under Low-Velocity Impact," *AIAA Journal*, Vol. 35, No. 9, 1997, pp. 1518–1521.

[4]Bathe, K. J., *Finite Element Procedures*, international ed., Prentice–Hall, Englewood Cliffs, NJ, 1996, Chap. 9.

[5]Hughes, T. J. R., Taylor, R. L., Sackman, J. L., Curnier, A., and Kanoknukulchai, W., "A Finite Element Method for a Class of Contact-Impact Problems," *Computer Methods in Applied Mechanics and Engineering*, Vol. 8, No. 3, 1976, pp. 249–276.

[6]Taylor, R. L., and Papadopoulos, P., "On a Finite Element Method for Dynamic Contact/Impact Problems," *International Journal for Numerical Methods in Engineering*, Vol. 36, No. 12, 1993, pp. 2123–2140.

[7]Chaudhary, A., and Bathe, K. J., "A Solution Method for Static and Dynamic Analysis of Three-Dimensional Contact Problems with Friction," *Computers and Structures*, Vol. 24, No. 6, 1986, pp. 855–873.

[8]Lee, K., "A Numerical Solution for Dynamic Contact Problems Satisfying the Velocity and Acceleration Compatibilities on the Contact Surface," *Computational Mechanics*, Vol. 15, No. 3, 1994, pp.189–200.

[9]Zienkiewicz, O. C., and Taylor, R. L., *The Finite Element Method*, 4th ed., McGraw–Hill, New York, 1991, Chap. 10.

[10]Hulbert, G. M., and Hughes, T. J. R., "Space–Time Finite Element Methods for Second-Order Hyperbolic Equations," *Computer Methods in Applied Mechanics and Engineering*, Vol. 84, No. 3, 1990, pp. 327–348.

[11]Johnson, C., "Discontinuous Galerkin Finite Element Methods for Second-Order Hyperbolic Problems," *Computer Methods in Applied Mechanics and Engineering*, Vol. 107, Nos. 1–2, 1993, pp. 117–129.

[12]Reddy, B. D., *Functional Analysis and Boundary-Value Problems: An Introductory Treatment*, Wiley, New York, 1986, Chap. 7.

[13]Adams, R. A., *Sobolev Spaces*, Academic, New York, 1975, Chap. 1.

[14]Kim, S. J., Cho, J. Y., and Kim, W. D., "From the Trapezoidal Rule to Higher Order Accurate and Unconditionally Stable Time Integration Method for Structural Dynamics," *Computer Methods in Applied Mechanics and Engineering*, Vol. 149, Nos. 1–4, 1997, pp. 73–88.

[15]Kim, S. J., and Cho, J. Y., "Penalized Weighted Residual Method for the Initial Value Problems," *AIAA Journal*, Vol. 35, No. 1, 1997, pp. 172–177.

[16]Oden, J. T., and Carey, G. G., *Finite Element, Vol. V: Special Problems in Solid Mechanics*, Prentice–Hall, Englewood Cliffs, NJ, 1984, Chap. 4.

[17]Zhong, Z. H., *Finite Element Procedures for Contact–Impact Problems*, Oxford Univ. Press, New York, 1993, Chap. 4.

S. Saigal
Associate Editor